Lawrence Berkeley National Laboratory

Title
Test of weak and strong factorization in nucleus-nucleus collisions atseveral hundred MeV/nucleon

Permalink
https://escholarship.org/uc/item/81q4c3w8

Authors
La Tessa, Chiara
Sihver, Lembit
Zeitlin, Cary
et al.

Publication Date
2006-06-21

Peer reviewed

Test of weak and strong factorization in nucleus-nucleus collisions at several hundred MeV/nucleon

C. La Tessa,[1, *] L. Sihver,[1, 2] C. Zeitlin,[3] J. Miller,[3] S. Guetersloh,[3]
L. Heilbronn,[3] D. Mancusi,[1] Y. Iwata,[4] and T. Murakami[4]

[1] *Nuclear Engineering, Applied Physics, Chalmers University of Technology, 412 96 Gothenburg, Sweden*
[2] *Department of Mathematics, Computer Science and Physics, Roanoke College, Salem, VA, USA*
[3] *Lawrence Berkeley National Laboratory, Berkeley, CA, USA*
[4] *Division of Accelerator Physics and Engineering National Institute of Radiological Sciences, Chiba, Japan*

Total and partial charge-changing cross sections have been measured for argon projectiles at 400 MeV/nucleon in carbon, aluminum, copper, tin and lead targets; cross sections for hydrogen were also obtained, using a polyethylene target. The validity of weak and strong factorization properties has been investigated for partial charge-changing cross sections; preliminary cross section values obtained for carbon, neon and silicon at 290 and 400 MeV/nucleon and iron at 400 MeV/nucleon, in carbon, aluminum, copper, tin and lead targets have been also used for testing these properties. Two different analysis methods were applied and both indicated that these properties are valid, without any significant difference between weak and strong factorization. The factorization parameters have then been calculated and analyzed in order to find some systematic behavior useful for modeling purposes.

I. INTRODUCTION

Heavy ions collisions at beam energies around a few hundred MeV/nucleon, well above the nuclear binding energy but below the energy at which resonance production becomes important, have distinct characteristics. Over the past three decades, fragmentation cross sections at these energies have been measured for many projectile-target combinations. In order to elucidate the underlying physics, it is useful to identify a systematic behavior in the fragmentation cross sections. One such behavior is factorization [1], a concept originally from high energy physics and subsequently extended to heavy ion interaction [2]. It states that at high enough beam energies the partial charge-changing cross section can be written as:

$$\sigma(P,T,F) = \sigma_P^F \gamma_{PT} \qquad weak\ factorization \qquad (1)$$

or

$$\sigma(P,T,F) = \sigma_P^F \gamma_T \qquad strong\ factorization \qquad (2)$$

$\sigma(P,T,F)$ is the fragmentation cross section for the projectile P incident upon the target T and producing the fragment F, σ_P^F is a factor depending only upon the projectile and the fragment while the target factors γ_{PT} and γ_T depend respectively upon the target and the projectile and only upon the target.

One important application of the factorization property is the rescaling procedure, which is the base of several cross section prediction models [3, 4]. Under the assumption that weak factorization holds, it is possible to write the fragmentation cross section as:

$$\sigma(P,T,F) = \sigma(P,\bar{T},F)\frac{\gamma_{P,T}}{\gamma_{P,\bar{T}}} \qquad (3)$$

where $\gamma_{P,T}$ and $\gamma_{P,\bar{T}}$ are the target factors for a specific target T and the reference target $\bar{T}$. The target factors are generally obtained using simple semi-empirical formulas (e.g. Eq. 11); the value of $\sigma(P,\bar{T},F)$ can be calculated with semi-empirical algorithms. In particular, the models discussed in [3] and [4] use hydrogen as a reference target, because of the large amount of target fragmentation cross sections measured for protons projectiles, that can be reversed as projectiles fragmentation cross sections on hydrogen target.

Weak factorization is also one of the basic predictions in the abrasion-ablation theory [5] and the investigation of its validity could therefore be useful for testing the goodness of this model.

In this work fragmentation cross sections have been measured for different projectile-energy-target combinations and analyzed in order to test if the data followed the factorization rules. We describe herein the analysis procedure for obtaining cross sections as well as the two methods, graphical and analytical, used for validating weak and strong factorization. The factorization parameters defined in Eq. 1 and 2 have been calculated; in particular the target factors have been fitted with appropriate equations in order to investigate their dependence upon the target mass number. Finally the results have been compared with data from literature.

II. EXPERIMENT DESCRIPTION

All the experiments have been performed at the Heavy Ion Medical Accelerator at Chiba (HIMAC) [6]; the projectiles, their kinetic energy at extraction from the accel-

*Corresponding author. E-mail address: chiara@nephy.chalmers. se; tel: +46 31 7722911; fax: +46 31 7723079.

erator and the year of the experiment are listed in Table 1.

Projectile (Z)	Kinetic energy (MeV/nucleon)	Year of the experiment
Carbon (6)	290	1997, 1998
Carbon (6)	400	1997, 1998
Neon (10)	290	2004
Neon (10)	400	2003
Silicon (14)	290	2004
Silicon (14)	400	1999, 2003
Argon (18)	400	2000
Iron (26)	400	1999

Table I: List of the projectiles used together with their energy and the year of the experiment.

The experimental setup for 400 MeV/nucleon argon (Figure 1), is typical.

Fully depleted lithium-drifted silicon detectors were used for particles identification. All the detectors were aligned on the beam axis and read out with standard electronics [7]. For each projectile partial and total charge changing cross sections were measured on carbon, polyethylene, aluminum, copper, tin and lead. All the targets used in the experiment had a natural composition and their thicknesses never exceeds 50% of the interaction length of the primary beam. Cross sections on hydrogen were obtained by subtracting the cross section for carbon from the cross section for polyethylene, appropriately weighted.

III. DATA ANALYSIS

A. Cross section measurement

The analysis was performed using the CERN library package *PAW* [8]. Our analysis method is based on the use of graphical cuts made on the detectors energy spectra and it has been described in a previous work [9]. For the present analysis we always chose the detectors pair closest to the target in order to maximize the angular acceptance, whose typical value was approximately $7°$.

The fluence for events with charge Z has been defined as:

$$\Phi(Z) = N(Z)/\sum_{Z=1}^{Z_{\text{primary}}} N(Z) \qquad (4)$$

where N(Z) is the number of particles produced per each charge. Corrections have been applied to take into account the attenuation of the beam in the detectors and the fragmentation in the parts of the experimental apparatus other than silicon (detectors dead layer, air, etc.). The fluence obtained after applying these correction is indicated as $\phi_{corr}(Z)$. A detailed description of the data analysis has been reported in a previous work [10].

The cross sections related to the probability for the projectile to change its charge when interacting with the target nuclei is called total charge-changing cross section and can be written as:

$$\sigma_{cc} = -\frac{A \ln \phi_{corr}(\text{primary})}{\rho d N_a}, \qquad (5)$$

where A is the target mass, ρ the target density, d the target thickness, N_a the Avogadro's number and $\phi_{corr}(primary)$ the corrected primary beam fluence. The cross section related to the probability for the projectile to produce a given fragment when interacting with the target nuclei is called partial charge-changing cross section and can be written as:

$$\sigma_z = \sigma_{cc}\frac{\phi_{corr}(Z)}{1 - \phi_{corr}(\text{primary})}. \qquad (6)$$

Charge-changing cross sections are, by definition, measured in target with infinitesimal depth: target thicknesses were then chosen to be sufficiently large to give reasonable statistics, but thin enough to keep the corrections for secondary nuclear interactions in the target reasonably small.

The measured cross sections were corrected in order to take into account the finite depth of the targets which gives a probability for the produced fragments to undergo higher-generation interactions. This correction will affect the fragment yields by increasing the number of fragments with charge close to the primary ions and decreasing the number of lighter fragments. The correction has been calculated using a Monte Carlo program that incorporates the NUCFRG2 nuclear fragmentation model [11]. Given the cross sections calculated by the model, and the beam and target characteristics, it is possible to model up to five generations of interactions. The calculated fragment yield per incident beam particle for each combination of fragment charge, target material and target thickness gives a correction which has been applied to the data. The corrections are typically on the order of half the fraction of an interaction length presented by the target to the primary. For example, for a target thickness of 20% of an interaction length, about 20% of the incident primaries undergo a charge-changing interaction in the target, and we therefore expect that about 10% of the fragments within a few charge units of the primary will undergo secondary charge-changing interactions. Assigning a 10% error to the NUCFRG2 charge-changing cross sections, the relative uncertainty in the correction in this instance is $(0.1 \cdot 0.1) = 0.01$, i.e. the correction introduces a 1% uncertainty into the final result. This is typically much smaller than the other uncertainties in the analysis.

The cross sections measured in different thicknesses of the same material were combined using standard methods for determining weighted averages. These average values are affected by two kinds of errors: a statistical one, which simply arises from the limited number of events, and a methodological one, which reflects the difference of the individual analysis procedures and is also
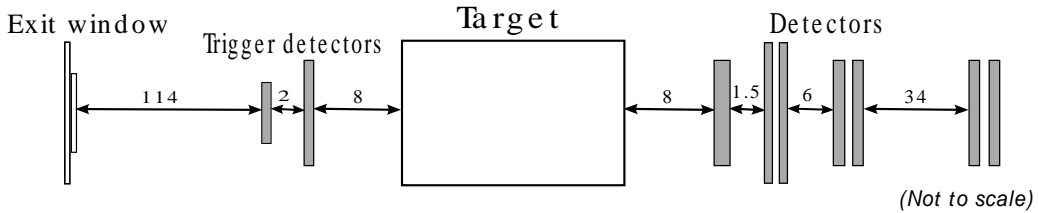
Figure 1: Scheme of a typical experimental setup chosen for the 2000 argon experiment (all distances are reported in cm).

related to the fact that the cross sections have been obtained using several target thicknesses. The first type of uncertainty is calculated using the error propagation method, while the second is determined by examination of the spread in measured cross sections obtained with different target depths. Since the statistical error is typically dominated by the methodological error, the latter can be taken as a reasonable estimation of the uncertainties on the average cross sections.

B. Cross sections

In Table II the total and partial charge-changing cross sections are listed for the argon projectile in all targets. Hydrogen cross sections have been calculated using the formula $\sigma(H) = 0.5[\sigma(CH_2) - \sigma(C)]$.

Silicon cross sections are reported in [12]; the cross sections for all the other projectiles are still preliminary data and therefore are not listed here but will be soon published in a separate paper.

IV. METHODS FOR TESTING THE FACTORIZATION PROPERTY

Two methods have been generally used for testing the factorization property: a graphical approach which gives a general idea of the data behavior and an analytical method which allows calculating the factorization parameters.

With the graphical method we check that:

- for any given projectile $\bar{P}$, and fragments F and F', the ratio $\frac{\sigma(\bar{P},T,F)}{\sigma(\bar{P},T,F')}$ is independent on the target T;

or, equivalently, that

- for any given projectile $\bar{P}$, fragment F and targets T and T', the ratio $\frac{\sigma(\bar{P},T,F)}{\sigma(\bar{P},T',F)}$ is independent on the fragment;

These two statements test the degree to which weak factorization holds. Moreover, if the second ratio is also independent on the projectile, strong factorization holds. Data for each projectile have been analyzed to verify

weak factorization while groups of two or three projectiles have been used to test strong factorization.

In the first case a reference target was chosen for each projectile and all the partial charge-changing cross sections relative to the other targets were divided by the reference value; for each target, then, these values were averaged over the fragments and the mean has been used as a normalization factor:

$$a_F = \frac{\sigma(\bar{P},T,F)/\sigma(\bar{P},T_{ref},F)}{\langle \sigma(\bar{P},T,F)/\sigma(\bar{P},T_{ref},F)\rangle_T}. \qquad (7)$$

The quantity $\langle \sigma(\bar{P},T,F)/\sigma(\bar{P},T_{ref},F)\rangle_T$ represents the mean value of the ratio $\sigma(\bar{P},T,F)/\sigma(\bar{P},T_{ref},F)$ for a fixed target T. If weak factorization held all the ratios should be around 1, independently on the fragment.

The graphical method for testing the strong factorization is the same than the one described above for the weak factorization, with the exception of the normalization factor which in this case is averaged over all the projectiles and fragments involved. If strong factorization held all the ratios should be around 1, independently on the fragment and the projectile.

The analytical method is based on the minimization of the χ^2 functions:

$$\chi_w^2 = \sum_T \sum_F \frac{[\sigma(P,T,F) - \sigma_P^F \gamma_{PT}]^2}{[\delta\sigma(P,T,F)]^2} \qquad (8)$$

for the weak factorization;

$$\chi_s^2 = \sum_P \sum_T \sum_F \frac{[\sigma(P,T,F) - \sigma_P^F \gamma_T]^2}{[\delta\sigma(P,T,F)]^2} \qquad (9)$$

for the strong factorization.

$\delta\sigma(P,T,F)$ represent the uncertainties on the cross section values $\sigma(P,T,F)$. Since the parameters are defined up to a multiplicative constant, we need to fix one of them in order to uniquely determine all the others; the value of one of the parameters was thus chosen to be 1.

The minimization has been performed using a program developed by our group that gave also the corresponding χ^2 value in the minimum. The algorithm chosen for the minimization process (Levenberg-Marquardt) provided an estimation of the coviariances matrix from which it was possible to calculate the parameter uncertainties.

Charge	H	C	Al	Cu	Sn	Pb
18	435±22	1268±63	1740±87	2493±125	3365±168	4319±216
17	126±13	191±19	212±21	271±27	343±34	406±41
16	100±10	136±14	161±16	205±20	241±24	277±28
15	62±6	100±10	128±13	154±15	168±17	218±22
14	61±6	108±11	128±13	164±16	215±21	247±25
13	30±3	80±8	99±3	124±12	161±16	211±21
12	16.0±1.6	87±9	101±10	125±12	168±17	170±17
11	16.4±1.6	54±5	80±8	85±8	106±11	110±11
10	9.6±1.0	58±6	72±7	97±10	113±11	154±15

Table II: Total and partial charge-changing cross sections (in mb) of 400 MeV/nucleon argon in all targets.

Together with the χ^2 values, another quantity, namely the discrepancy d, has been used to test the goodness of the fit:

$$d(P,T,F) = \frac{|\sigma_{meas}(P,T,F) - \sigma_{calc}(P,T,F)|}{\sigma_{meas}(P,T,F)} \quad (10)$$

where $\sigma_{meas}(P,T,F)$ are the measured cross sections and $\sigma_{calc}(P,T,F)$ the cross sections calculated according to Eq. 1 and 2 using the parameters obtained by the regression. This ratio gives an idea of how close the calculated cross sections are to the measured ones and then how good the fit is. For each projectile the discrepancy values have been averaged over all the fragments and targets and the results have been used for testing weak factorization; strong factorization, instead, was validated using the discrepancies averaged also over all the projectiles.

Figure 2: a_F values of all fragments for argon projectile in aluminum; copper was used as a reference target.

A. Graphical method results

In figures 2 and 3 the a_F values (Eq. 7) for the argon projectile are plotted for all the fragments in aluminum and lead targets respectively. In both cases copper target has been chosen as a reference since it has a mass number in between the two targets. In Figures 4 and 5 the a_F values are plotted for neon projectiles at 290 MeV/nucleon and 400 MeV/nucleon as a function of the charged fragments, again for aluminum and lead targets. In the former case the data were used to test weak factorization, in the latter to test strong factorization. In all the plots the line at $a_F = 1$ is the line on which the point would lie if factorization held exactly.

While the graphical method does not allow extraction of the factorization parameters, it nevertheless represents a useful tool for understanding the systematic of the cross sections: the results reported in Figures 2-5 show that there is little or no differences between the plots testing weak and strong factorization. Moreover both aluminum and lead targets seem to conform quite well to the factorization property; a similar behavior can be found for all the other projectile-target pairs with the exception of hydrogen (discussed below).
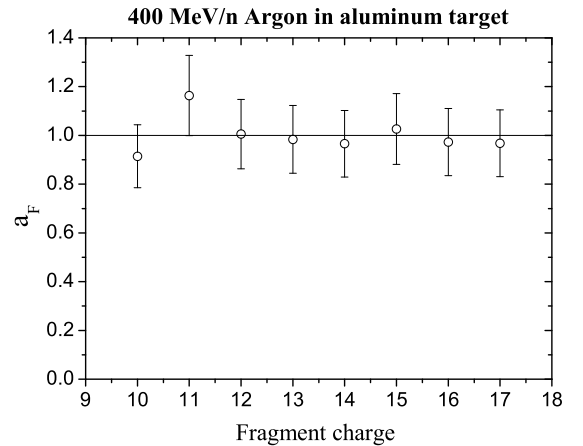

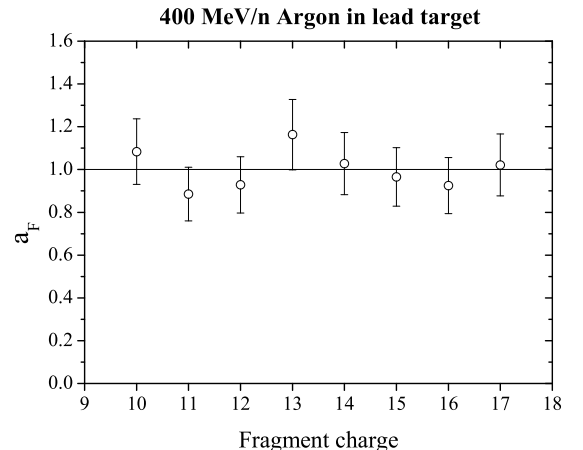Figure 3: a_F values of all fragments for argon projectile in lead; copper was used as a reference target.

Neon in aluminum target
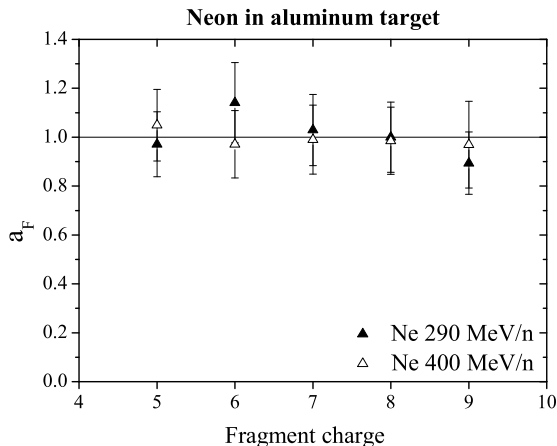
Figure 4: a_F values of all fragments for neon projectiles in aluminum; copper was used as a reference target.
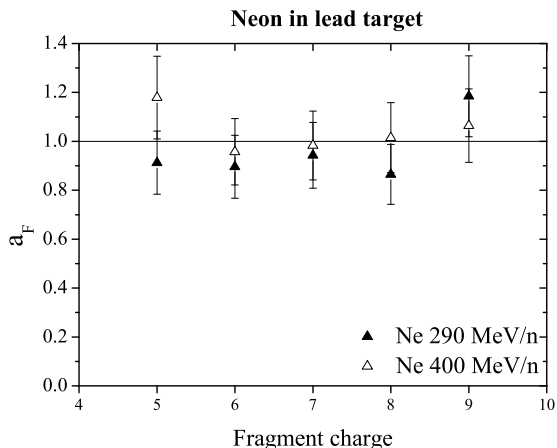

Neon in lead target

Figure 5: a_F values of all fragments for neon projectiles in lead; copper was used as a reference target.

B. Analytical method results

The results obtained with the minimization of the χ^2_w and χ^2_s functions (Eq. 8 and 9) are summarized in Tables III and IV respectively. For each single projectile (weak factorization test) and group of projectiles (strong factorization test), the kinetic energy, the charge of the fragments cross sections used, the χ^2 value obtained from the fit, the degrees of freedom and the respective p-value are reported as well as the average discrepancy and the percentage of the discrepancies lower than 5% and 10%. The minimization process included all the measured cross sections except the ones relative to the hydrogen target.

Mn ions (Z=25) were not included in the iron analy-

sis because it has been observed [13] that this fragment can be produced with either fragmentation or electromagnetic dissociation of the primaries, and therefore does not follows the factorization rules. The parameters obtained from all the regressions are reported in appendix.

Two methods have been chosen for testing the hypothesis of factorization: the χ^2 and the average discrepancy. The former tests the goodness of the fit, i.e. if the data show a factorization trend within their uncertainties. For this reason its value is very sensitive to outliers and to the errors in the cross sections and, if the latter are very small, the former can be very large. It is nevertheless possible that the data follow the factorization rules to some approximation, with discrepancies larger than the experimental uncertainties, but still small enough to consider the concept of factorization a useful one for developing semi-empirical systematics. Consideration of the results obtained with this test can only prove if factorization does or does not hold exactly but no further conclusion can be drawn. If we wish, instead, to test whether or not factorization properties can be fruitfully used to predict fragmentation cross sections to some accuracy, then the χ^2 test is not suitable. The average discrepancy (Eq. 10), on the other hand, does not depend explicitly on the data errors (see Eq. 10) and it simply measures how well the calculated cross sections approach the measured ones: even if the agreement is not within the stated uncertainties, the factorization properties shown from the experimental data could still be useful for predicting cross sections.

The χ^2 results reported in Tables III and IV show suspiciously high p-values for all projectiles; this is due to the fact that the cross sections used for the test are preliminary data and have therefore large uncertainties (around 10%) which lead to unrealistically small χ^2 values. This result suggests that the χ^2 test is indeed overly sensitive to the data uncertainties and that it might not be the most suitable choice for checking the validity of factorization. On the other hand, if we look at the average discrepancies we can observe that, for both singles and grouped projectiles, these values never exceed 7% and their overall average is 4%; we could therefore say that the factorization rules hold within a given uncertainty, which is small enough to justify the use of this properties for modelling purposes.

It is also important to notice that with both the χ^2 and the discrepancy test, there is no indication of the fact that strong factorization cannot explain the data. In particular, the values of the average discrepancies for weak and strong factorization have a same mean value of 4%, with a lowest value around 2% and a highest value around 7%. The percentages of calculated cross sections are always higher than 45% for a discrepancy up to 5%, and always higher than 75% for a discrepancy up to 10%. These results strongly suggest that the experimental data obey strong factorization independent on the projectile, the energy and the target chosen. However our study is limited to the heavy fragments: the cross sections of frag-

Projectile	Energy (MeV/nucleon)	Fragments involved	χ_w^2	df	p-value (%)	Average discrepancy (%)	< 5% (%)	< 10% (%)
C	290	3-5	1.8	8	99	2.8	80	100
C	400	3-5	0.89	8	100	1.8	100	100
Ne	290	5-9	13	16	68	5.3	60	80
Ne	400	5-9	6	16	99	3.6	84	92
Si	290	7-13	13	24	96	3.9	71	94
Si	400	7-13	37	24	4	4.0	80	94
Ar	400	10-17	12	28	100	4.3	72	90
Fe	400	13-24	44	44	47	6.8	47	78

Table III: Results obtained from the minimization of the χ_w^2 function (Eq. 8) and values of the average discrepancy (discrepancy d (Eq. 10) averaged over all the targets for all singles projectiles).

Projectile	Energy (MeV/nucleon)	Fragments involved	χ_s^2	df	p-value (%)	Average discrepancy (%)	< 5% (%)	< 10% (%)
C-C	290-400	3-5	2.9	20	100	2.4	87	100
Ne-Ne	290-400	5-9	21	36	98	4.8	64	80
Si-Si	290-400	7-13	53	52	45	4.2	74	93
Ar-Fe	400-400	13-17	32	36	67	6.1	54	82
Ar-Si-Si	400-290-400	10-13	47	44	34	5.1	60	87
Ne-Ne-Si-Si	290-400-290-400	7-9	29	44	96	4.7	63	85

Table IV: Results obtained from the minimization of the χ_s^2 function (Eq. 9) and values of the average discrepancy (discrepancy d (Eq. 10) averaged over all the targets and projectiles) for all grouped projectiles.

ments with charge lower than about half of the primary cannot be accurately determined with the leading particle analysis we performed [9] and therefore they cannot be used for testing factorization. Additional analysis of the data obtained with small-acceptance detectors may provide further insight about this point.

C. Parameters dependence on uncertainties in the data

The factorization parameters are directly related to the data uncertainties (see Eq. 8 and 9) and therefore it is important to investigate their dependence on the errors.

For this purpose the uncertainties have been randomly generated from a minimum value of 1% to a maximum value of 50%. These values, together with the measured cross sections, were used to minimize the χ^2 function and to obtain the factorization parameters. This process was repeated 1000 times and, for each parameter, a standard deviation and a relative standard deviation (the standard deviation divided by the mean value) were calculated. The same quantities were obtained by changing the maximum error value to 40%, 30%, 20%, 10%, 7%, 5% and 3%. The average relative standard deviations of the fragment factors σ_P^F as a function of the maximum error values are reported in Figure 6 for 290 MeV/nucleon silicon and the group of 400 MeV/nucleon argon and 400 MeV/nucleon iron; in Figure 7 the average relative standard deviations of the target factors (γ_{PT} for 290 MeV/nucleon silicon and γ_T for the group of argon and iron) are plotted for the same projectiles.
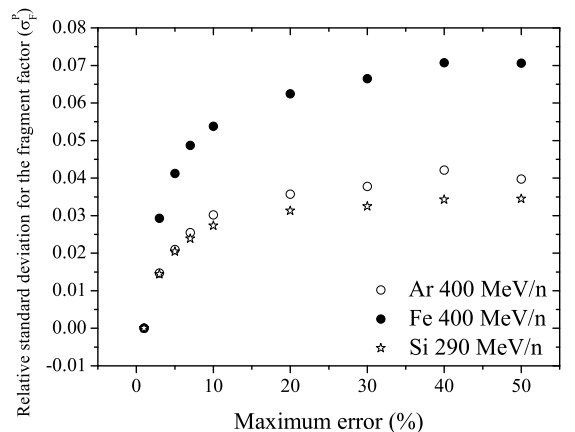
The plots show that, for both parameters, the relative

Figure 6: Average relative standard deviations of the fragment factors (σ_P^F) as a function of the maximum error values for 290 MeV/nucleon silicon and the group of argon 400 MeV/nucleon and iron 400 MeV/nucleon.

standard deviations never exceed 10%, even for an unrealistic maximum error of 50%: this means that the factorization parameters are rather insensitive to variation in the uncertainties. For example, data sets with same cross section measurements but different errors, with values between 1% and 10% (as in our case), will provide factorization parameters with a spread of a few percent; in general factorization parameters obtained with different data sets will show small variations even if the cross sections uncertainties show an unrealistic maximum value
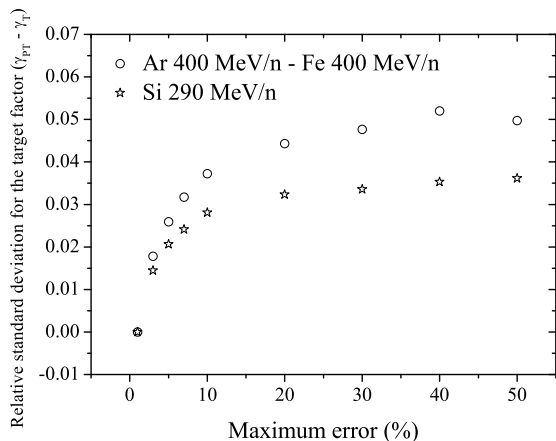
Figure 7: Average relative standard deviations of the target factors (γ_P^T- γ_T) as a function of the maximum error values for 290 MeV/nucleon silicon and the group of argon 400 MeV/nucleon and iron 400 MeV/nucleon.

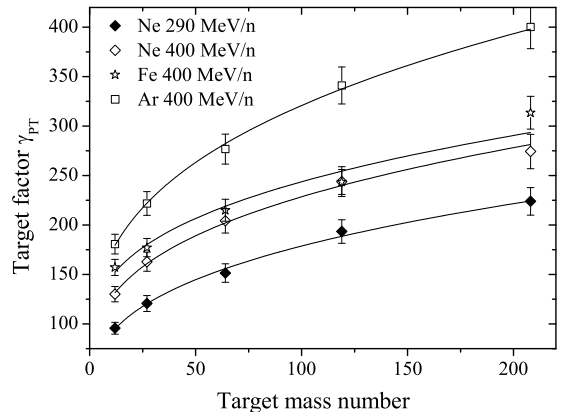Figure 8: γ_{PT} values plotted as a function of the target mass and fitted according to Eq. 11 for single projectiles.

of 50%.

## D. Analysis of the target factor

The dependence of the target factor on the target mass number has been investigate in order to find a systematic trend of the data: this would allow us to obtain the factorization parameters for a given target without measuring cross sections. A previous work [14] suggests that good expressions for all target factors are:

$$\gamma_{PT} = a(A_T^{1/3} + A_P^{1/3} - b) \tag{11}$$

$$\gamma_T = cA_T^e \tag{12}$$

where a, b, c, d and e are adjustable parameters. These equations were used to fit the target factors of the single and grouped projectiles respectively; the data with their corresponding fit lines are reported in Figures 8 and 9 for single projectiles, and in Figures 10 and 11 for grouped projectiles.

All the parameters obtained from the fits, together with the corresponding χ^2 values and p-values, are reported in Table V for the single projectiles and in Table VI for the grouped projectiles.

In all cases, except for the iron projectile (both single and grouped with argon), the p-values are higher than 40%, meaning that the data are well-fitted by Eq. 11 and 12. The parameters obtained from the fits can be used to estimate the cross sections; the comparison between these values and the measured cross sections will be the topic of a further work.
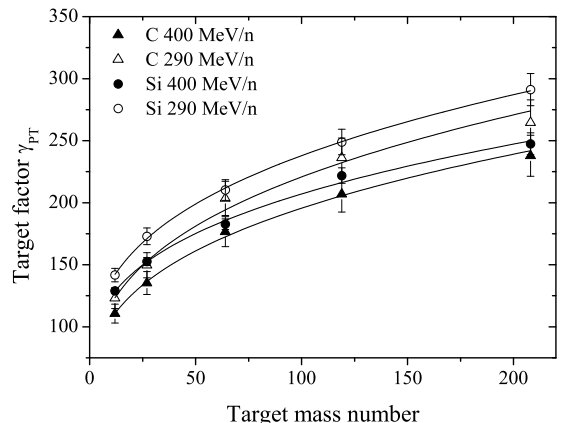
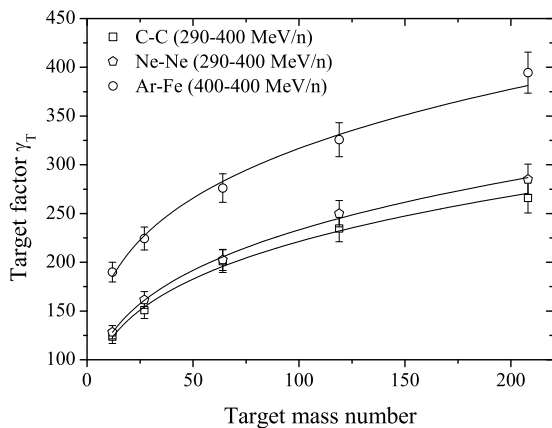

Figure 9: γ_{PT} values plotted as a function of the target mass and fitted according to Eq. 11 for single projectiles.

Projectile (energy MeV/nucleon)	a	b	χ^2	p-value (%)
C (290)	41±4	66±26	0.87	83
C (400)	36±4	54±23	2.0	57
Ne (290)	41±4	74±26	0.35	95
Ne (400)	35±3	83±20	0.40	94
Si (290)	41±3	74±19	0.12	99
Si (400)	33.3±1.7	49±10	1.4	71
Ar (400)	60±5	164±37	0.20	98
Fe (400)	39±4	84±30	2.6	43

Table V: Target factors obtained by fitting each single projectile data set with Eq. 11.

Projectile (energy MeV/nucleon)	c	e	χ^2	p-value (%)
C-C (290-400)	62±6	0.28±0.03	0.49	92
Ne-Ne (290-400)	63±6	0.28±0.02	0.24	97
Si-Si (290-400)	79±5	0.294±0.015	1.0	79
Ar-Fe (400-400)	99±10	0.0.25±0.02	0.99	80
Ar-Si-Si (400-290-400)	47±4	0.24±0.02	1.3	73
Ne-Ne-Si-Si (290-400-290-400)	71±6	0.25±0.02	0.34	79

Table VI: Target factors obtained by fitting each group of projectile data set with Eq. 12.
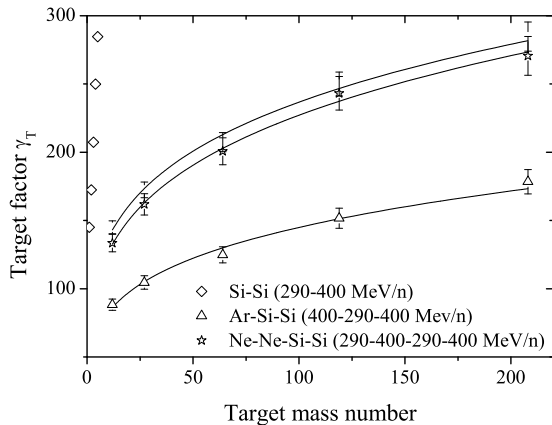
Figure 10: γ_T values plotted as a function of the target mass and fitted according to Eq. 12 for grouped projectiles.

Figure 11: γ_T values plotted as a function of the target mass and fitted according to Eq. 12 for grouped projectiles.

E. The hydrogen target

The results obtained for hydrogen, using both the graphical and the analytical methods, lead to conclude that this target does not obey the factorization laws expressed in Eq. 1 and 2. In Figure 12 the a_F values are plotted against the fragments charge for argon 400 MeV/nucleon, while in Figure 13 the same quantities are plotted for neon 290 MeV/nucleon and neon 400 MeV/nucleon. The first plot is obtained with the graphical procedure for testing the weak factorization, the latter with the procedure for testing the strong one; in all cases copper has been used as a reference target.
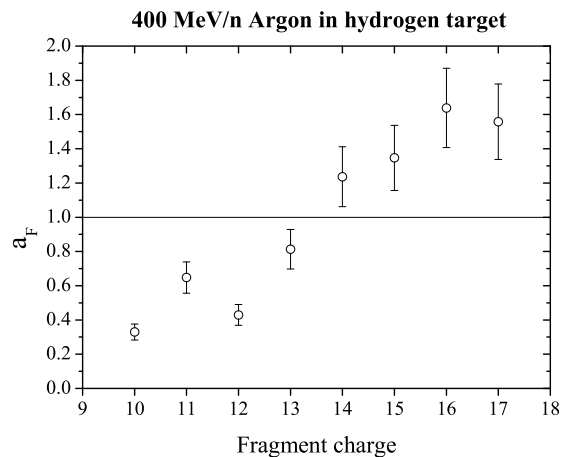
Figure 12: a_F values of all fragments for argon projectile in hydrogen; copper has been used as a reference target.

Both figures show that, for each projectile, the a_F values have a same trend, decreasing with decreasing fragments charge. This behavior has been observed for all the projectiles and it is thus clear that factorization does not apply to collision in hydrogen target. Further evidence is shown in Table VII where the results from the minimization of the χ^2_w function (Eq. 8), performed including the hydrogen cross sections, are reported for the 400 MeV/nucleon argon projectile.

If we compare these results with the ones reported in Table III for argon, we can observe that both the χ^2_w value and the average discrepancy are much higher when the hydrogen data are included in the fit. Moreover in this case the average discrepancy exceeds 10% while all the other values, obtained from the fits which did not include the hydrogen cross sections, were below 7%.
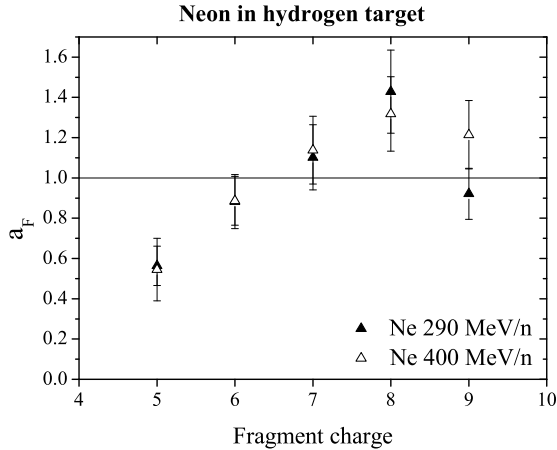
Figure 13: a_F values of all fragments for neon projectile in hydrogen; copper has been used as a reference target.

Fragments involved	χ_w^2	df	p-value (%)	Average discrepancy (%)	< 5% (%)	< 10% (%)
10-17	197	35	< 0.1	13	37	62

Table VII: Results obtained from the minimization of the χ_w^2 function (Eq. 8) for the 400 MeV/nucleon argon projectile, including the hydrogen cross sections.

The fact that the hydrogen target does not follow the factorization rules has been already observed and can be found in literature [14, 15].

V. COMPARISON WITH PREVIOUS WORKS

Previous factorization studies have been focused on the validation of this property within the uncertainties and have therefore chosen the χ^2 method as the most appropriate for this aim. In reference [14] it was proved, with this method, that weak factorization holds while strong factorization is violated; in this case the cross section errors were on average smaller than 10%, but, as our results pointed out, the χ^2 is not a reliable method because of its strong sensitility to the data uncertainties. Moreover in [14] the test was performed only on three projectiles, a too small number to provide a stringent evidence of the validity of the χ^2 as a suitable test.

It might also be important to point out two main differences between [14] and the present work: the projectiles energies and the experimental setup. It has been observed that partial charge-changing cross sections show factorization properties which improve with increasing projectile energy; in the present work all the projectiles used had a maximum energy of 400 MeV/nucleon, a much lower value than the energies chosen in [14], which were at least 1 GeV/nucleon. Moreover, with the experimental setup in [14], it was possible to measure isotopic cross sec-

tions and investigate if each of the isotopes followed the factorization rules; in this experiment we were only able to distinguish particles with different charge. It is possible that, for a given charge, not all the isotopes factorize because other processes, such as electromagnetic dissociation, can contribute [16]. If this effect is big enough for the cross sections to deviate from the factorization behavior beyond the uncertainties, the χ^2 value will dramatically increase because of its high sensitivity to the outliers.

In both [14] and our works, information about strong factorization could not be gathered with the χ^2. In the former the deviation of the data from strong factorization has not been quantified; in the present work, on the other hand, the uncertainties on the cross sections were too large to give reasonable results with the the χ^2 and therefore an alternative test (the average discrepancy) has been used for this purpose.

In reference [17] it is shown that both weak and strong factorization hold for light and medium heavy fragments ($Z \leq 8$ for Fe and Kr and $Z \leq 34$ for Xe) while they are violated for fragments with higher charge. The deviations of these cross sections from the factorization trend have not been quantified since only the χ^2 was used as a testing approach.

The discrepancy for light fragments between these results and those presented in this paper could be once again explained by the choice of the projectiles energy (1 GeV/nucleon) and the experimental setup (nuclear emulsions rather than silicon detectors): our analysis technique, in fact, does not allow measurement of the correct cross sections for light fragments and therefore it is not possible to check if factorization hold for these particles. Nonetheless, the fact that light fragments do not show any significant difference between weak and strong factorization is consistent with the behavior of the heavy fragments observed in our results.

VI. CONCLUSIONS

In this paper we investigated the factorization concept using fragmentation cross sections measured for different projectile-energy-target combinations at energies of several hundred MeV/nucleon. Two approaches, graphical and analytical, have been chosen for testing this property and were applied to all the measured cross sections. The graphical method gave strong indication of the fact that all the data followed factorization and that there was not a significant difference between weak and strong factorization (see Eq. 1 and Eq. 2). The analytical method, based on the minimization of the χ^2 functions (Eq. 8 and Eq. 9), provided the values of the factorization parameters expressed in Eq. 1 and Eq. 2. This approach gave different results depending on which method was chosen for testing the goodness of the fit: the χ^2 test didn't produced realistic results due to the large uncertaities on the cross sections while the average discrepancy (Eq. 10)

proved that this property can be useful for cross section prediction purposes. In fact the disagreement between measured and calculated (using the factorization parameters) cross sections was around 4%, which can be a satisfactory result from a modeling point of view. These results pointed out that the χ^2 might not be the most suitable choice for testing factorization, due also to its strong dependence from the data uncertainties and from its sensitivity to outliers.

According to the average discrepancy all the projectile-target pairs show factorization behavior except for the hydrogen target, which strongly deviates from this property; the same conclusion can be found in literature [14, 15].

Since the the factorization parameters are directly related to the data uncertainties (see Eq. 8 and Eq. 9), their dependence from the cross sections error have been investigated. Considering maximum uncertainties from 1% to 50% of the data, the corresponding factorization parameters show a disagreement which never exceeds 10%: this result allowed us to conclude that the parameters are robust against incorrect estimation of the uncertainties.

Appendix: FACTORIZATION PARAMETERS

The factorization parameters obtained from the regressions are reported in Tables XIV-XVII for all the projectiles, single and grouped.

290 MeV/nucleon C projectile

Charge	σ_P^F	Target	γ_{PT}
5	1	C	123±8
4	0.40±0.02	Al	150±10
3 or 2He	1.40±0.09	Cu	203±14
		Sn	236±16
		Pb	265±18

Table VIII: Weak factorization parameters for 290 MeV/nucleon carbon.

400 MeV/nucleon C projectile

Charge	σ_P^F	Target	γ_{PT}
5	1	C	111±8
4	0.42±0.03	Al	135±9
3 or 2He	1.54±0.10	Cu	177±12
		Sn	207±14
		Pb	238±17

Table IX: Weak factorization parameters for 400 MeV/nucleon carbon.

290 MeV/nucleon Ne projectile

Charge	σ_P^F	Target	γ_{PT}
9	1	C	130±8
8	1.07±0.07	Al	163±10
7	0.92±0.06	Cu	204±12
6	1.09±0.07	Sn	244±15
5	0.63±0.04	Pb	274±17

Table X: Weak factorization parameters for 290 MeV/nucleon neon.

400 MeV/nucleon Ne projectile

Charge	σ_P^F	Target	γ_{PT}
9	1	C	96±6
8	1.46±0.010	Al	121±8
7	1.14±0.07	Cu	151±9
6	1.42±0.09	Sn	193±12
5	0.68±0.05	Pb	224±14

Table XI: Weak factorization parameters for 400 MeV/nucleon neon.

290 MeV/nucleon Si projectile

Charge	σ_P^F	Target	γ_{PT}
13	1	C	142±5
12	1.10±0.05	Al	173±6
11	0.64±0.03	Cu	210±8
10	0.63±0.03	Sn	248±10
9	0.355±0.017	Pb	291±13
8	0.70±0.03		
8	0.58±0.03		

Table XII: Weak factorization parameters for 290 MeV/nucleon silicon.

400 MeV/nucleon Si projectile

Charge	σ_P^F	Target	γ_{PT}
13	1	C	129±2
12	1.08±0.03	Al	153±3
11	0.614±0.015	Cu	183±4
10	0.653±0.015	Sn	222±6
9	0.347±0.010	Pb	247±9
8	0.723±0.019		
7	0.579±0.017		

Table XIII: Weak factorization parameters for 400 MeV/nucleon silicon.

400 MeV/nucleon Ar projectile

Charge	σ_P^F	Target	γ_{PT}
17	1	C	181±10
16	0.72±0.05	Al	222±12
15	0.54±0.03	Cu	277±15
14	0.60±0.04	Sn	341±19
13	0.46±0.03	Pb	400±22
12	0.46±0.03		
11	0.306±0.019		
10	0.34±0.02		

Table XIV: Weak factorization parameters for 400 MeV/nucleon argon.

400 MeV/nucleon Fe projectile

Charge	σ_P^F	Target	γ_{PT}
24	1	C	157±8
23	0.71±0.05	Al	177±9
22	0.63±0.04	Cu	215±11
21	0.52±0.03	Sn	243±13
20	0.50±0.03	Pb	314±17
19	0.42±0.03		
18	0.37±0.02		
17	0.33±0.02		
16	0.35±0.02		
15	0.30±0.02		
14	0.35±0.02		
13	0.32±0.02		

Table XV: Weak factorization parameters for 400 MeV/nucleon iron.

290 Mev/nucleon C - 400 MeV/nucleon C projectiles

Charge	σ_P^F (C 290)	σ_P^F (C 400)	Target	γ_T
5	1	0.89±0.06	C	124±7
4	0.40±0.02	0.37±0.02	Al	151±9
3 or 2He	1.40±0.09	1.37±0.09	Cu	201±12
			Sn	235±13
			Pb	266±15

Table XVI: Strong factorization parameters for 290 MeV/nucleon and 400 MeV/nucleon carbon.

290 Mev/nucleon Ne - 400 MeV/nucleon Ne projectiles

Charge	σ_P^F (Ne 290)	σ_P^F (Ne 400)	Target	γ_T
9	1	0.76±0.05	C	128±7
8	1.06±0.07	1.11±0.07	Al	161±9
7	0.92±0.06	0.87±0.06	Cu	202±11
6	1.08±0.07	1.08±0.07	Sn	250±14
5	0.62±0.04	0.51±0.03	Pb	285±16

Table XVII: Strong factorization parameters for 290 MeV/nucleon and 400 MeV/nucleon neon.

290 Mev/nucleon Si - 400 MeV/nucleon Si projectiles

Charge	σ_P^F (Si 290)	σ_P^F (Si 400)	Target	γ_T
13	1	0.89±0.03	C	145±5
12	1.10±0.05	0.96±0.03	Al	172±6
11	0.64±0.03	0.54±0.02	Cu	207±7
10	0.63±0.03	0.58±0.02	Sn	250±8
9	0.354±0.017	0.307±0.012	Pb	285±11
8	0.70±0.03	0.64±0.02		
7	0.58±0.03	0.51±0.02		

Table XVIII: Strong factorization parameters for 290 MeV/nucleon and 400 MeV/nucleon silicon.

400 Mev/nucleon Ar - 400 MeV/nucleon Fe projectiles

Charge	σ_P^F (Ar 400)	σ_P^F (Fe 400)	Target	γ_T
17	1	0.263±0.017	C	190±10
16	0.72±0.05	0.277±0.018	Al	224±12
15	0.54±0.03	0.236±0.015	Cu	276±15
14	0.60±0.04	0.281±0.018	Sn	326±17
13	0.46±0.03	0.256±0.016	Pb	394±21

Table XIX: Strong factorization parameters for 400 MeV/nucleon argon and 400 MeV/nucleon iron.

400 MeV/nucleon Ar - 290 Mev/nucleon Si - 400 MeV/nucleon Si projectiles

Charge	σ_P^F (Ar 400)	σ_P^F (Si 290)	σ_P^F (Si 400)	Target	γ_T
13	1	1.64±0.09	1.46±0.07	C	88±4
12	1.00±0.06	1.80±0.10	1.58±0.08	Al	105±5
11	0.67±0.04	1.05±0.06	0.90±0.04	Cu	125±6
10	0.73±0.05	1.04±0.06	0.95±0.05	Sn	152±7
				Pb	178±9

Table XX: Strong factorization parameters for 400 MeV/nucleon argon, 290 MeV/nucleon silicon and 400 MeV/nucleon silicon.

	290 MeV/nucleon Ne - 400 Mev/nucleon Ne - 290 MeV/nucleon Si - 400 MeV/nucleon Si projectiles					
Charge	σ_P^F (Ne 290)	σ_P^F (Ne 400)	σ_P^F (Si 290)	σ_P^F (Si 400)	Target	γ_T
9	1	0.77±0.05	0.37±0.02	0.32±0.02	C	133±6
8	1.07±0.07	1.12±0.07	0.74±0.04	0.68±0.03	Al	162±8
7	0.93±0.06	0.87±0.06	0.61±0.04	0.55±0.03	Cu	201±10
					Sn	243±12
					Pb	271±14

Table XXI: Strong factorization parameters for 290 MeV/nucleon neon, 400 MeV/nucleon neon, 290 Mev/nucleon silicon and 400 MeV/nucleon silicon.

[1] W. R. Frazer, L. Ingber, C. H. Mehta, C. H. Poon, D. Silverman, K. Stowe, P. D. Ting, and H. J. Yesian, Rev. Mod. Phys. **44**, 284 (1972).

[2] J. Cugnon and R. Sartor, Phys. Rev. C **21**, 2342 (1980).

[3] L. Sihver, C. H. Tsao, R. Silberberg, T. Kanai, and A. F. Barghouty, Phys. Rev. C **47**, 1225 (1993).

[4] C. H. Tsao, R. Silberberg, A. F. Barghouty, L. Sihver, and T. Kanai, Phys. Rev. C **47**, 1257 (1993).

[5] J. Hüfner, K. Schäfer, and B. Schürmann, Phys. Rev. C **12**, 1888 (1975).

[6] Y. H. *et. al.*, Tech. Rep., NIRS (1992).

[7] C. Zeitlin, K. A. Frankel, W. Gong, L. Heilbronn, E. J. Lampo, R. Leres, J. Miller, and W. Schimmerling, Radiat. Meas. **23**, 65 (1994).

[8] R. Brun, O. Couet, C. Vandoni, and P. Zanarini, Comput. Phys. Commun. **57**, 432 (1989).

[9] C. Zeitlin, A. Fukumura, L. Heilbronn, Y. Iwata, J. Miller, and T. Murakami, Phys. Rev. C **64**, 024902 (2001).

[10] C. L. Tessa, S. Guetersloh, L. Heilbronn, J. Miller, L. Sihver, and C. Zeitlin, Adv. Space Res. **35**, 223 (2005).

[11] C. Zeitlin, L. Heilbronn, J. Miller, S. E. Rademacher, T. Borak, T. R. Carter, K. A. Frankel, W. Schimmerling, and C. E. Stronach, Phys. Rev. C **56**, 388 (1997).

[12] C. Zeitlin, A. Fukumura, S. B. Guetersloh, L. Heilbronn, Y. Iwata, J. Miller, and T. Murakami, submitted to Nuclear Physics (2005).

[13] G. D. Westfall, L. W. Wilson, P. J. Lindstrom, H. J. Crawford, D. E. Greiner, and H. H. Heckman, Phys. Rev. C **19**, 1309 (1979).

[14] D. L. Olson, B. L. Berman, D. E. Greiner, H. H. Heckman, P. J. Lindstrom, and H. J. Crawford, Phys. Rev. C **28**, 1602 (1983).

[15] G. Iancu, F. Flesch, and W. Heinrich, Radiat. Meas. **39**, 525 (2005).

[16] D. L. Olson, B. L. Berman, D. E. Greiner, H. H. Heckman, P. J. Lindstrom, G. D. Westfall, and H. J. Crawford, Phys. Rev. C **24**, 1529 (1981).

[17] M. I. Adamovic, E. S. Basova, M. M. Chernyavsky, A. Dirner, and K. G. Gulamov, Europhys. Lett. **50**, 441 (2000).